J. Water Environ. Nanotechnol., 3(1): 40-50 Winter 2018

ORIGINAL RESEARCH PAPER

Acid-thermal Activated Nanobentonite as an Economic Industrial Adsorbent for Malachite Green from Aqueous Solutions. Optimization, Isotherm, and Thermodynamic Studies

Reza Tayebee**, *Vahid Mazruy

Department of Chemistry, Hakim Sabzevari University, Sabzevar, Iran

Received: 2017.10.16 Accepted: 2018.01.12 Published: 2018.01.30

ABSTRACT

The limited adsorption capacity of natural clays is a crucial and economic issue which confined their applications in industry as cheap adsorbents to remove toxic contaminants from wastewaters. Here, the adsorption capacity of a natural nano bentonite was enhanced by a simple acid and thermal activation and the manufactured nano-adsorbent was characterized by FESEM, BET, FT-IR, and XRD. Effects of pH, temperature, sorbent capacity, and the initial concentration of malachite green were examined. The isotherm behavior of the adsorption system was investigated by the Langmuir and Freundlich isotherm models. Also, the kinetic inspections demonstrated that the adsorption of malachite green matched with the pseudo-second-order kinetic and the obtained thermodynamic parameters H, S, and G showed that the adsorption of malachite green was a spontaneous and endothermic process. The results indicated that the acid-thermal activated nano bentonite, with an enhanced surface area of >220 m^2/g, can be depleted as a powerful and low-cost adsorbent to expel malachite green from aqueous solutions.

Keywords: *Adsorption, Isotherm, Malachite Green, Nanobentonite, Removal, Thermodynamic*

How to cite this article

Tayebee R, Mazruy V. Acid-thermal Activated Nanobentonite as an Economic Industrial Adsorbent for Malachite Green from Aqueous Solutions. Optimization, Isotherm, and Thermodynamic Studies. J. Water Environ. Nanotechnol., 2018; 3(1): 40-50.
DOI: 10.22090/jwent.2018.01.004

INTRODUCTION

Numerous enterprises, such as textile, material, pharmaceutics, printing, pulp and paper, plastics, and iron-steel industries discharge a lot of highly colored effluents which can be extremely lethal even at low concentrations and are one of the significant reasons for environmental pollution [1-4]. Considering their chemical structures, dyes are resistant substances in nature and are biologically non-degradable; accordingly, hard to decolorize once discharged into the aquatic environment. These mutagenic and cancer-causing agents can bring about extreme harms to the central nervous system, brain, liver, the kidneys, and reproductive system [4-6]. These days, disposal of pharmaceutical wastes and lethal reactive organic dyes has raised concerns about health, hygiene, and sanitation among the regulators including the water suppliers and the common public. Such a situation has rendered immense necessity to ensure removal of pharmaceutical wastes before discharge of both municipal and industrial effluents. Albeit, a few costly strategies including coagulation, flocculation, precipitation, oxidation, membrane filtration, ozonation, photocatalysis, and ultrasound irradiation are performed to eliminate poisons from wastewaters [7-13], however, liquid-phase adsorption of dyes into the surface of an appropriate adsorbent is a potent, simple, and flexible strategy which has gained favor in recent years [4, 14].

* Corresponding Author Email: *rtayebee@hsu.ac.ir.*

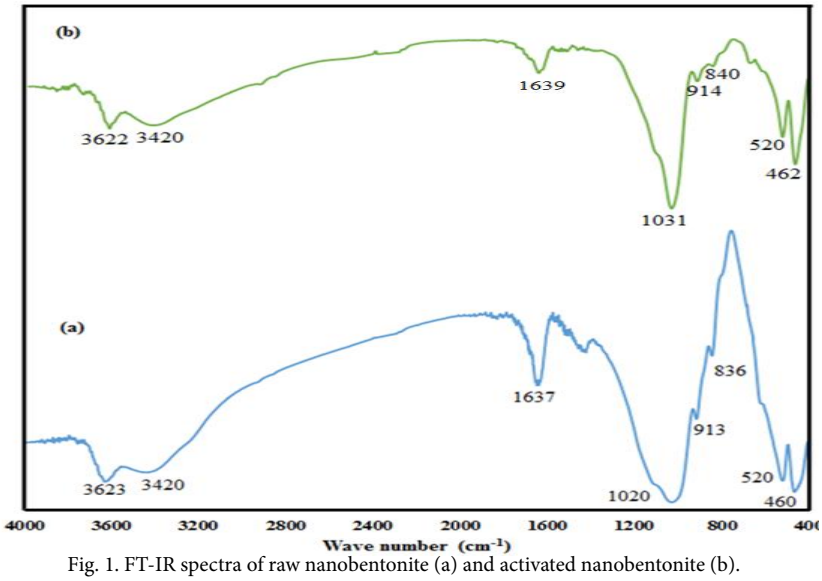

Fig. 1. FT-IR spectra of raw nanobentonite (a) and activated nanobentonite (b).

Meanwhile, most common adsorbents have fundamental disadvantages, such as high cost of treatment and troublesome recovery which expands the cost of wastewater treatment [14, 15]. Along these lines, there is a need to discover low-cost, locally accessible, and renewable materials as sorbents for colored wastes. Among different adsorbents, distinctive types of bentonite, as montmorillonite clay, procured prominence and provided an extraordinary position and has been widely utilized because of its large adsorption capacity, porous structure, good surface area, high mechanical and chemical stability, and high surface reactivity [16, 17]. Bentonite is comprised of one Al octahedral sheet positioned between the tetrahedral coordinated layers of silicon ions [18]. The isomorphs exchange of Al^{3+} for Si^{4+} in the tetrahedral sheet and Mg^{2+} for Al^{3+} in the octahedral layer brings about a net negative surface charge on the bentonite. This charge irregularity is balanced by convertible cations such as Na^{+} and Ca^{2+} at the bentonite surface [19, 20]. The layered arrangement of clay can be broadened after moistening. Na^{+} and Ca^{2+} are firmly hydrated in the presence of water, providing a hydrophilic surrounding at the bentonite surface [17, 21]. In conclusion, although bentonite has a total unbiased charge, it has an excessive negative charge on its cross-section, showing a strong affinity for hetero-aromatic cationic dyes.

In order to study increment of adsorption capacity of natural clays, an easily accessible and low-cost nano bentonite was chosen and the adsorption capacity was upgraded by a simple subsequent acid and thermal initiation. Then, the improved nanoclay was documented for the elimination of the acid dye malachite green. Malachite green (MG), is an N-methylated diamino triphenyl methane cationic dye which has been generally utilized for the coloring of wool, leather, jute, silk, and as a fungicide and biocide in aquaculture industry [17, 22]. MG is deeply cytotoxic to living cells and furthermore behaves as a liver tumor-enhancing agent [23].

EXPERIMENTAL

Material and methods

All substances and beginning materials were provided by Merck and Fluka and were utilized without additional purification. The clay handled in this study is hydrophilic nano bentonite acquired from Sigma-Aldrich. Nanobentonite was refined by washing carefully with distilled water to wipe out external impurities and dried at 105 °C. Malachite green was acquired from Sigma-Aldrich and utilized as received. Ultraviolet-visible spectra were archived with a Photonix UV-Vis Array Spectrophotometer. The X-ray diffraction patterns acquired from an XPert MPD diffractometer with Cu K_{α} radiation at 40 keV and 30 mA, and the scanning rate was set to 3° min^{-1} in the 2θ range of 5° to 80°. The morphology and spreading of particles were considered by field emission scanning electron microscopy (FESEM) using a KYKY-EM3200 with an accelerating voltage of 26 kV and HITACHI S-4160, individually. A freeze dryer (Model FD-

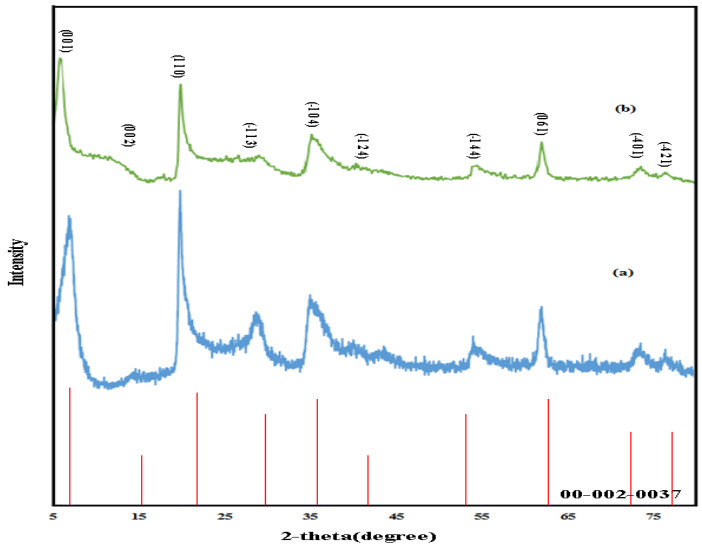

Fig. 2. XRD patterns of raw (a) and activated nanobentonite (b).

10, Pishtaz Equipment Engineering Co, Iran) was utilized for drying of the nano bentonite samples. BET-specific surface areas were specificated by nitrogen adsorption with Belsorp II (BEL Japan, Inc). Infrared spectra were recorded on KBr pellets on an 8400 Shimadzu Fourier transform spectrophotometer.

Acid and thermal activation of nano bentonite

The acid-thermal activation of nano bentonite was followed by a two-step methodology. Primarily, bentonite was enacted utilizing 0.1 M HCl at 30 °C and stirred for 1 h. Then, the acidified nano bentonite was washed with excess double-ionized water. The samples were comprehensively washed until Cl^- ions were imperceptible while pH 5 was kept up. The acidified nano bentonite was then exposed to thermal activation by calcination at 100 °C for 120 min in a muffle furnace. The samples were cooled in a desiccator and put away in air-tight plastic bottles for further use.

Preparation of the adsorbate solutions

Malachite green used was of commercial quality and utilized without further purification. The thorough information of MG is given in Table S1. Dye stock solution (500 mgl^{-1}) was made by solving precisely weighed amount of the dye in deionized water. Experimental dye solution of various concentrations was prepared by diluting the stock solution with the appropriate volume of deionized water.

Adsorption experiments

Batch adsorption analyses were performed by equilibrating 0.01 g of the adsorbent with 50 ml aqueous solution of the dye with the required concentration (20-120 mgl^{-1}) at 25 °C and pH of 6 for 60 min. After 10 min, the suspension was centrifuged and concentration of malachite green adsorbed on the nano bentonite was investigated by UV-Vis at the wavelength of 619 nm. The amount of the dye adsorbed on the nano bentonite was ascertained utilizing Eq. (1):

$$q_e = \frac{(C0 - Ce).V}{M} \quad (1)$$

Where, C_0 and Ce are the primary and final concentrations of the dye (mgl^{-1}), respectively. V is the volume of the solution (lit), and M is the weight of the used nano bentonite (g) [24].

Cation exchange capacity (CEC) measurements by $[Cu(en)_2]^{2+}$

CEC was calculated according to the announced procedure [25]. A solution of $CuSO_4$ (200 ml, 1M) was prepared by dissolving 31.9 g of $CuSO_4$ (0.2 mol) in distilled water. A solution of ethylenediamine (500 ml, 1M) was set up by dissolving 30.05 g (33.4 ml, 0.5 mol) of ethylenediamine in deionized water. The complex was made by adding 10 ml of the $CuSO_4$ solution to 20 ml of the ethylenediamine solution. The trivial excess of the amine ensured the quantitative formation of the complex. The solution was diluted with water to 1000 ml of $[Cu(en)_2]^{2+}$

Table 1. Surface area and pore volume for nanobentonite and acid/thermal activated nanobentonite.

Clay	Surface area (m^2/g)	Total pore volume (cm^3/g)
Nanobentonite	63	16
Acid/thermal activated nanobentonite	226	53

solution (0.01 M, pH 8.1). The concentration of copper complex was determined by photometry at the absorption maximum of 548 nm. For the CEC determination, 100 mg of the dried clay was transformed to 25 ml centrifugal tubes and 8 ml of the 0.01 M complex solution $[Cu(en)_2]^{2+}$ was added. The samples were shaken for 30 min; after that, centrifuged at 3000 rpm for 10 min. Then, 3 ml of the supernatants were transferred into cuvettes, and the absorption was measured at 548 nm for $[Cu(en)_2]^{2+}$ using calibration curves. The amount of copper complex adsorbed was ascertained from the concentration differences. The CEC for nano bentonite was acquired as 143 mEq/g.

RESULT AND DISCUSSION

FT-IR studies

Fig. 1 demonstrates FT-IR spectra of natural and altered bentonite. The bands at 520 and 752 cm^{-1} can be credited to Si–O–Al symmetric vibrations. The peaks at 836 and 912 cm^{-1} correspond to Al-Mg–OH bending vibrations. The OH stretching vibration and Si–O bending are appeared at 3623 and 1037 cm^{-1}, individually. Similar peaks were appeared in bentonite clay [26]. The stretching vibrations of OH originating from Al-OH and Si–OH bands were seen at 3709 cm^{-1}. The envelope at ~3630 cm^{-1} belonged to H-bonded water stretching with a shoulder close to 3420 cm^{-1}, due to the overtone of water bending vibration at ~1639 cm^{-1}. The peaks at 1020-10310cm^{-1} were appointed to the characteristic groups of silicates which were mostly identified with the stretching vibrations of M–O (where M = Si, Al) within the range of 1100-1040 cm^{-1} and 400-1200 cm^{-1}; While, the bands at ~520 and 460 cm^{-1} were due to Al–O–Si and Si–O– Si bending vibrations, separately. The peak at 914 cm^{-1} was responsible for Al-Al-OH group deformation [27].

XRD pattern

The XRD patterns of the raw and adjusted nano bentonite appear in Fig. 2. As shown in Fig. 2, the XRD pattern displayed diffraction lines of a high crystalline nature at 2θ= 7.4, 15, 19.9, 30, 35, 54.2, 62.3, 73.4 and 76.8°, which corresponds to (100), (200), (011), (31-1), (40-1), (44-1), (160), (10-4) and (12-4) crystal planes, respectively, matched well with the JCPS of 00-002-0037 confirming the formation of montmorillonite structure. Moreover, no impurity peaks were observed, confirming the high purity of the sample. The comparison of XRD of raw and activated nano bentonite demonstrated that no new peaks were observed after modification by acid-thermal technique. The average crystallite sizes of raw and activated nano bentonites were specified by the X-ray line broadening method utilizing the Scherrer equation, Eq. 2 [28].

$$D=0.94\lambda/\beta_D \cos\theta \quad (2)$$

Where D is the particle size in nanometers, λ is the wavelength of the radiation (1.54056 A° for Cu-K_α radiation), θ is the peak position and β_D is the peak width at the half-maximum intensity. By this strategy, the average crystallite sizes of the raw and activated nano bentonite were accomplished 26 and 27 nm, respectively.

Adsorption of nitrogen

N_2 adsorption/desorption isotherms of the prepared untreated and acid/thermal activated nano bentonites are observed in Fig. S1 and the corresponding textural characterization results are shown in Table 1. The surface area of the unactivated nano bentonite was low, but acid-thermal activated nano bentonite showed significant addition to porosity and surface area. The V_a of the activated clay revealed an increase in the region of $P/P_o = 0$, showing that the clay has micropores. Moreover, a hysteresis is detected in the region above $P/P_o = 0.5$, implicating that the activated clay has mesopores.

FESEM investigations

The activated nano bentonite was inspected using FESEM to analyze its morphological characteristics. Here, the FESEM images of the activated nano bentonite are displayed in Fig. 3. The FESEM image of the activated nano bentonite indicated that the interlayer sites may have been collapsed, bringing about more tightly-bound structure. It seems that the acid activation eventuated leaching refinement of cations, making the clay surface more porous as confirmed by BET analysis.

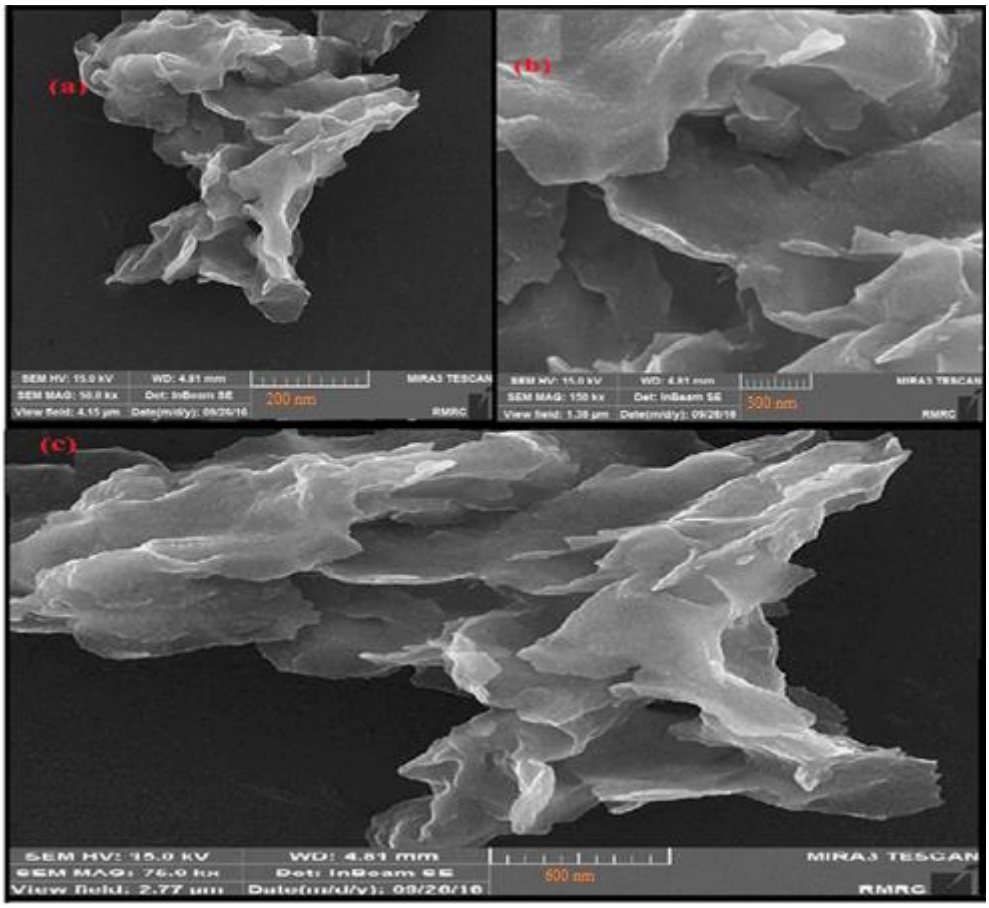

Fig. 3. FESEM images of activated nanobentonite.

Effects of the operating parameters

Effect of the adsorbent dose

The adsorbent dose is an imperative factor affecting sorption and defines the sorption capacity of the adsorbent for a given initial concentration of the adsorbate. Fig. 4 demonstrates the adsorption profile of MG vs adsorbent concentration in the range of 1-15 mg. It was observed that the rate of the color removal expanded with enhancing the adsorbent dosage, because of increasing the surface area and accessibility of more active adsorption sites [29]. Noteworthy, uptake of the dye was enhanced with increasing the adsorbent dose, the equilibrium adsorption capacity for MG was diminished with increasing the quantity of the adsorbent. This finding would be due to a lessening of the total adsorption surface area available for the dye molecules eventuating from overlap or aggregation of the adsorption sites [30, 31]. In this way, with increasing the adsorbent mass, the amount of the dye adsorbed onto the unit mass of the adsorbent was reduced; thus, bringing about a decrease in qe with increasing the adsorbent mass concentration. Further, maximum dye removal (99%) was achieved at 10 mg adsorbent dose and further growth in the adsorbent dose did not essentially change the adsorption yield, because of the binding of approximately all dye molecules onto the adsorbent surface and foundation of the equilibrium among the dye molecules on the adsorbent and in the solution [32]. The optimized adsorbent dose was observed to be 10 mg and used for the progressive experiments.

Effect of pH

The pH of the adsorbate is the most imperative parameter that determines the amount of MG adsorbed. Fig. 5 indicates that just a low amount of MG adsorption occurred at the pH of 5 and this amount remained almost constant beyond pH 5. Increase in the amount of adsorbate relies upon the properties of the adsorbent surface and the dye structure. At acidic pH, the surface charge of clay may be positive, in this way making H^+ ions

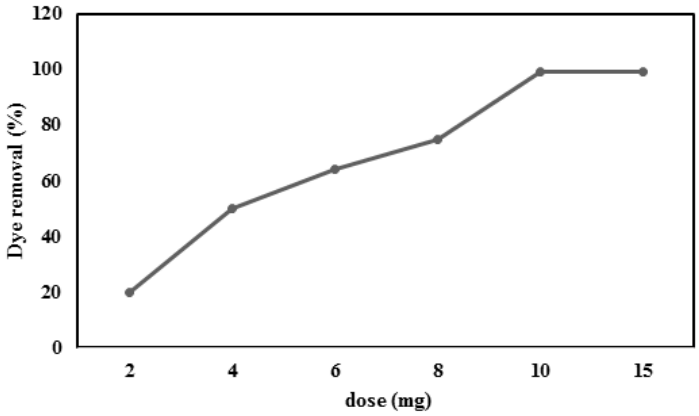

Fig. 4. Effect of the adsorbent dose on the adsorption of MG by nanobentonite. Conditions: initial dye concentration: 40 mgl^{-1}, pH: 6.0, T: 303 K, contact time: 100 min.

compete strongly with the cationic dye and cause a reduction in the amount of the dye elimination. At higher pH, the external surface of the acid-thermal activated nano bentonite may be negatively charged; thus, improved sorption of the positively charged MG. Comparable results have been reported for sorption of MG onto Montmorillonite clay [24]. In this manner, pH 6 was picked as the ideal for subsequent adsorption studies.

Effect of initial MG concentration

Effect of initial dye concentration on the adsorption limit was examined in 20, 40, 60, 80, 100, and 120 mgl^{-1} at 303 K at a steady starting pH of 6, and 0.01 g of the adsorbent. The acquired outcomes demonstrated that the adsorption capacity was developed with increasing initial dye concentration (Fig. 6). When MG concentration was increased from 20 to 120 ppm, the amount of the adsorbed MG raised from 99 to 350 mg/g. Fig. 6 also indicates that the adsorption of MG was fast at the primary stages, and after that, it became slower. The reason would be due to the large number of vacant surface sites accessible for the adsorption during the initial stages of the treatment; while, after a lapse of time, the remaining surface sites hard to be involved due to repulsive forces among the MG adsorbed on the surface of nano bentonite and the solution phase [33]. It is clear that the adsorption process was dependent upon the initial concentration of the dye solution.

Effect of temperature

The effect of temperature on adsorption of MG was investigated at 303, 313, 323, and 333 K at pH of 6, 0.01 g of the adsorbent, and the initial MG 40 mgl^{-1}. The results are exhibited in Fig. S2. A slight increase in the removal and adsorption capacity was observed with enhancing temperature. The uptake of MG was increased as the temperature was raised from 303 to 333 K [34]. The q_e was calculated as 150, 170, 175 and 177 mgg^{-1} at 303, 313, 323 and 333 K, respectively. As the temperature increases, the kinetic energy of the dye molecules in solution also enhances to make the maximum number of the dye molecules reach the adsorbent surface [24]. At higher temperatures, the intensity of the border sheet thin down, because of the raised trend of the dyes to draw to the acid-thermal nano bentonite surface, which results in a diminish in adsorption as temperature enhances. Enhancing MG removal at higher temperatures would be due to the fact that the adsorption of MG was an endothermic procedure [35]. Increasing temperature was also appropriate for the mass carrying process by improving the propulsive force of MG molecules onto the clay and diminishing the energy obstruction of the reaction between the adsorbent and the adsorbate.

Adsorption Kinetics

Design of an adsorption system in the industry needs full data on the rate of adsorption as well as the rate determining step and adsorption kinetics which can be controlled by various types of mechanisms like film diffusion, pore diffusion, complexation, and ion-exchange processes [36]. Pseudo-first-order and pseudo-second-order kinetic models have been applied in the adsorption studies. The pseudo-first-order kinetic model

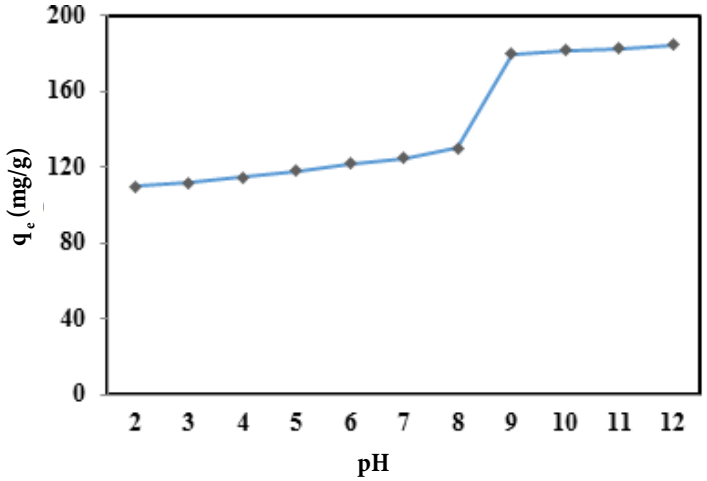

Fig. 5. Effect of pH on the adsorption of MG by the acid-thermal activated nanobenonite. Experimental conditions: initial dye concentration: 40 mgl^{-1}, dose 0.01 g, T: 303 K, contact time: 100 min.

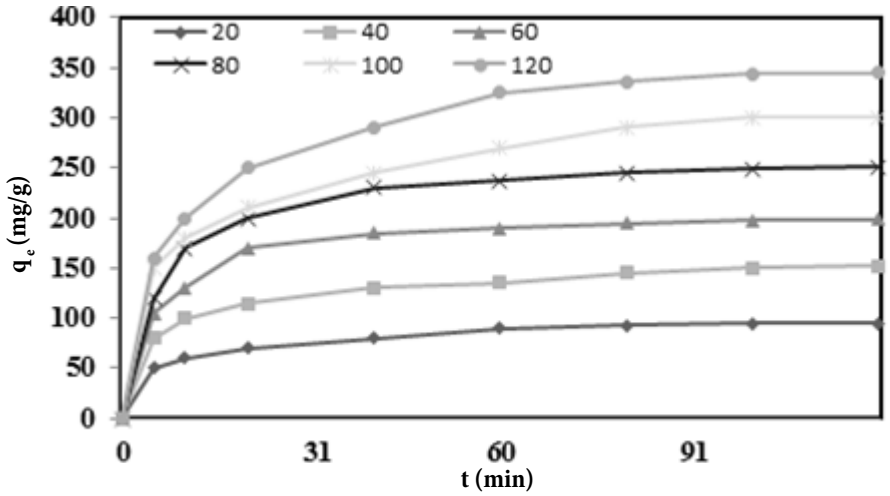

Fig. 6. Effect of initial dye concentration on the adsorption capacity of nanobentonite. Conditions: dose 0.01 g, pH: 6, T: 303 K.

assumes that the adsorption rate is proportional to the number of free adsorption sites. This kinetic pattern is equivalent to the diffusion expression captured for the diffusion via a boundary liquid film [37, 38]. The linear form of the pseudo-first-order rate equation is shown in Eq. 3.

$$\log(q_e - q_t) = \log q_e - \frac{K1}{2.303} \times t \qquad (3)$$

Where, q_e and q_t are the amount of MG adsorbed (mgg^{-1}) at equilibrium and at a given time (min.), respectively, and k_1 is the pseudo-first order rate constant min^{-1} [39]. A direct line plot of log ($q_e - q_t$) *vs* t provides k_1 and q_e from the slope and intercept, individually, (Figs. S3-S4). The rate constants and correlation coefficients for the pseudo-first order plots are listed in Table S2. In spite of the fact that the plots indicated good linearity with $R_2 \geq 0.98$, the $q_{e,\,cal.}$ and $q_{e,\,exp.}$ values are not in agreement with each other. Therefore, one can presume that the adsorption of MG did not follow pseudo-first-order kinetics. The decrease of the rate constants with enhancing MG concentration is a sign of the stiffer competition for adsorption locations in MG molecules [38].

The pseudo-second-order equation concerns that chemisorption is the rate determining step and

is expressed as given by Eq. 4:

$$\frac{t}{q_t} = \frac{1}{h} + \frac{t}{q_e} \quad (4)$$

Where, $h = k_2 q_e^2$ can be viewed as the initial adsorption rate ($g.mg^{-1}\ min^{-1}$) as t_0, and k_2 is the rate constant ($g.mg^{-1}\ min^{-1}$) of the pseudo-second-order adsorption [40]. The plot of t/q_t *vs* t should give a straight line if pseudo-second-order kinetics are pertinent and q_e, k_2, and h can be specified from the slope and intercept catch of the plot, respectively. A better linearity of the plots was acquired in our study by exerting the pseudo-second-order model compared to the pseudo-first-order model with $R_2 \geq 0.99$, as detailed in Table S2.

It is worth specifying that, the $q_{e,cal.}$ and $q_{e,exp.}$ values were practically comparable at all concentrations discussed. These findings displayed that the rate determining step phase was similar to the chemisorption due to sharing or replacing of the electrons between the adsorbate and the adsorbent. Generally, the pseudo-second-order rate constant, k_2, was reduced as the concentration of MG was increased because of the difficult competition for the adsorption sites as further MG molecules were present in the solution. Although, the initial adsorption rate, h, indicated an inverse pattern. A large number of adsorption sites available on the nano bentonite surface might reason a rapid adsorption of MG at higher concentrations, possibly due to the increase in the driving force of mass transfer and allowing MG molecules to reach the adsorbent surface in a shorter time.

Adsorption isotherms

Adsorption isotherm is an expression that indicates the relation between the quantity of adsorbate adsorbed per unit weight of adsorbent (qe, $mg.g^{-1}$) and the concentration of adsorbate in the solution bulk (Ce, $mg.l^{-1}$) at a certain temperature under equilibrium conditions. An adsorption isotherm is very helpful to provide data on the adsorption mechanisms, surface properties, and adsorbate-adsorbent interactions. The afforded plot was the Langmuir type adsorption isotherm in the Giles classification system (Fig. S5). The L-type isotherm usually confirms the chemical adsorption (chemisorption) and reflects a relatively great affinity between adsorbate and adsorbent. The equilibrium adsorption data were fitted to the two general isotherm patterns which are Langmuir and Freundlich, given by Eqs. 5 and 6, respectively.

$$\frac{C_e}{q_e} = \frac{1}{k.q_{max}} + \frac{C_e}{q_{max}} \quad (5)$$

$$lnq_e = lnk_f + \frac{1}{n}.lnC_e \quad (6)$$

Where, C_e is the equilibrium MG concentration ($mg.l^{-1}$), q_e is the amount of MG adsorbed at equilibrium ($mg.g^{-1}$), q_{max} is the maximum adsorption capacity (mgg^{-1}), b is the Langmuir constant (lmg^{-1}), K_F represents the Freundlich constant (mgg^{-1}) and n is discussed as the heterogeneity of the adsorbent surface and its tendency for the adsorbate [41,42]. The isotherm constants and correlation coefficients obtained from both patterns are exhibited in Table 2. It was found that the Freundlich model was the best-proportioned model for MG adsorption, which proposed that the adsorbent surface was heterogeneous in nature. The maximum adsorption capacity distinguished from the Langmuir isotherm was 312.5 mgg^{-1}. The "n" value was larger than unity, a proof that the bond amongst MG and the acid-thermal treated nano bentonite was strong. An examination of MG adsorption capacity of the acid-thermal nano bentonite beads with the previously utilized adsorbents is shown in Table 2. With a maximum adsorption of 312.5 mgg^{-1}, the nano bentonite is clearly a very impressive and promising adsorbent for the removal of MG from aqueous solutions.

Thermodynamic parameters of adsorption

The adsorption isotherm information observed at various temperatures were used to compute the important thermodynamic factors such as changes in Gibbs energy ΔG° ($kJ.mol^{-1}$), enthalpy change ΔH° ($kJ.mol^{-1}$) and entropy change ΔS° ($J.mol^{-1}K^{-1}$). The free energy of the adsorption process considering the adsorption equilibrium constant K_0 is given by the accompanying Eqs. 7-9:

$$\Delta G^\circ = -RT\, lnK_0 \quad (7)$$

$$\Delta G^\circ = \Delta H^\circ - T\Delta S^\circ \quad (8)$$

$$lnK_0 = -\frac{\Delta H^\circ}{RT} + \frac{\Delta S^\circ}{R} \quad (9)$$

Where T is the temperature in a unit of Kelvin and R defined as 8.314 $J.mol.K^{-1}$[27]. The values of ΔH° and ΔS° were obtained from the slope and intercept of the plot of lnK_0 against 1/T (Fig. S6) is listed in Table 3. When ΔG is positive, the reverse

Table 2. Langmuir and Freundlich isotherm constants and their correlation coefficients.

Langmuir			Freundlich		
q_{max} (mg.g^{-1})	b (l.mg^{-1})	R^2	K_f (mg.g^{-1})	n	R^2
312.5	42933	0.86	89.12	2.81	0.96

Table 3. Thermodynamic parameters for the adsorption of MG onto the nanobentonite surface.

T (k)	lnK_d	ΔG° (KJ/mol)	ΔH° (kj/mol)	ΔS° (j/mol)
303	2.7	-4.46	2.52	21.16
313	3.33	-3.89	2.52	21.16
323	3.55	-4.31	2.52	21.16
333	3.64	-4.52	2.52	21.16

reaction is spontaneous. When ΔG is negative, the forward reaction is spontaneous, and when ΔG is zero, the system has attained an equilibrium state [27]. Positive values of ΔH° and ΔS° propose an endothermic reaction, while the negative values of free energy change (ΔG°) showed that the adsorption is spontaneous (Table 3). The positive values of ΔS° suggested the developed randomness at the solid–solution interface during desorption of malachite green oxalate onto the nano bentonite surface [43].

CONCLUSION

Bentonite has been known as a cheap adsorbent over the last few decades due to its local and abundant availability and the modification capability. Activated nano bentonite with increased surface area >220 m^2g^{-1} has been considered as a good adsorbent for the expulsion of malachite green oxalate from aqueous solutions. In addition, studies are planned to raise the adsorption capacity of the nano bentonite by a simple and economic thermal and acid activation. Some vital factors such as pH, adsorbent dosage, contact time, initial dye concentration and temperature were also studied on the adsorption capacity (q_e). In this work, the equilibrium analysis indicated that Freundlich isotherm is fitted better to the adsorption data, suggesting that the MG does not form a monolayer on the adsorbent and rather pursues multilayer adsorption. The adsorption kinetics followed the pseudo-second-order kinetic model indicating chemisorption. Besides, higher adsorption capacity with growing temperature affirmed that the adsorption process was chemical in nature, spontaneous and endothermic as confirmed by assessment of the relevant thermodynamic parameters, *viz.* ΔG°, ΔH°, and ΔS°. It is additionally observed that acid-thermal activated nano bentonite can be used as a low-cost, promptly accessible, and easily prepared sorbent for the effective elimination of MG from aqueous solutions.

ACKNOWLEDGEMENTS

This work has been supported by the Center for International Scientific Studies & Collaboration (CISSC). Partial financial support from the Research Council of Hakim Sabzevari University is also greatly appreciated. .

CONFLICT OF INTEREST

The authors declare that there are no conflicts of interest regarding the publication of this manuscript.

SUPPLEMENTARY MATERIAL

The Supplementary Material for this article can be found online at: http://jwent.net/

REFERENCES

1. Xu M, McKay G. Removal of Heavy Metals, Lead, Cadmium, and Zinc, Using Adsorption Processes by Cost-Effective Adsorbents. In: Bonilla-Petriciolet A, Mendoza-Castillo DI, Reynel-Ávila HE, editors. Adsorption Processes for Water Treatment and Purification. Cham: Springer International Publishing; 2017. p. 109-38.
2. Lee KE, Morad N, Teng TT, Poh BT. Reactive Dye Removal Using Inorganic–Organic Composite Material: Kinetics, Mechanism, and Optimization. J Dispersion Sci Technol. 2014;35(11):1557-70.
3. Srivastava S, Sinha R, Roy D. Toxicological effects of malachite green. Aquat Toxicol. 2004;66(3):319-29.
4. Ahmad R, Kumar R. Adsorption studies of hazardous malachite green onto treated ginger waste. J Environ Manage. 2010;91(4):1032-8.

5. Özcan A, Özcan AS. Adsorption of Acid Red 57 from aqueous solutions onto surfactant-modified sepiolite. J Hazard Mater. 2005;125(1):252-9.

6. Jiang F, Dinh DM, Hsieh Y-L. Adsorption and desorption of cationic malachite green dye on cellulose nanofibril aerogels. Carbohydr Polym. 2017;173(Supplement C):286-94.

7. Verma AK, Dash RR, Bhunia P. A review on chemical coagulation/flocculation technologies for removal of colour from textile wastewaters. J Environ Manage. 2012;93(1):154-68.

8. Sadri Moghaddam S, Alavi Moghaddam MR, Arami M. Coagulation/flocculation process for dye removal using sludge from water treatment plant: Optimization through response surface methodology. J Hazard Mater. 2010;175(1):651-7.

9. Demirbas E, Kobya M. Operating cost and treatment of metalworking fluid wastewater by chemical coagulation and electrocoagulation processes. PROCESS SAF ENVIRON. 2017;105(Supplement C):79-90.

10. Zhu X, Zheng Y, Chen Z, Chen Q, Gao B, Yu S. Removal of reactive dye from textile effluent through submerged filtration using hollow fiber composite nanofiltlration membrane. Desalin Water Treat. 2013;51(31-33):6101-9.

11. Berberidou C, Kitsiou V, Lambropoulou DA, Antoniadis A, Ntonou E, Zalidis GC, et al. Evaluation of an alternative method for wastewater treatment containing pesticides using solar photocatalytic oxidation and constructed wetlands. J Environ Manage. 2017;195(Part 2):133-9.

12. Giannakis S, Liu S, Carratalà A, Rtimi S, Talebi Amiri M, Bensimon M, et al. Iron oxide-mediated semiconductor photocatalysis vs. heterogeneous photo-Fenton treatment of viruses in wastewater. Impact of the oxide particle size. J Hazard Mater. 2017;339(Supplement C):223-31.

13. Soltermann F, Abegglen C, Tschui M, Stahel S, von Gunten U. Options and limitations for bromate control during ozonation of wastewater. Water Res. 2017;116(Supplement C):76-85.

14. Crini G. Non-conventional low-cost adsorbents for dye removal: A review. Bioresour Technol. 2006;97(9):1061-85.

15. Ghaedi M, Hossainian H, Montazerozohori M, Shokrollahi A, Shojaipour F, Soylak M, et al. A novel acorn based adsorbent for the removal of brilliant green. DESALINATION. 2011;281(Supplement C):226-33.

16. Al-Asheh S, Banat F, Abu-Aitah L. Adsorption of phenol using different types of activated bentonites. Sep Purif Technol. 2003;33(1):1-10.

17. Arellano-Cárdenas S, López-Cortez S, Cornejo-Mazón M, Mares-Gutiérrez JC. Study of malachite green adsorption by organically modified clay using a batch method. Appl Surf Sci. 2013;280(Supplement C):74-8.

18. Manohar DM, Noeline BF, Anirudhan TS. Adsorption performance of Al-pillared bentonite clay for the removal of cobalt(II) from aqueous phase. Appl Clay Sci. 2006;31(3):194-206.

19. Anirudhan TS, Ramachandran M. Removal of 2,4,6-trichlorophenol from water and petroleum refinery industry effluents by surfactant-modified bentonite. J Water Process Eng. 2014;1(Supplement C):46-53.

20. Faghihian H, Mohammadi MH. Surface properties of pillared acid-activated bentonite as catalyst for selective production of linear alkylbenzene. Appl Surf Sci. 2013;264(Supplement C):492-9.

21. Ullah Z, Hussain S, Gul S, Khan S, Bangash FK. Use of HCl-modified bentonite clay for the adsorption of Acid Blue 129 from aqueous solutions. Desalin Water Treat. 2016;57(19):8894-903.

22. Alderman DJ. Malachite green: a review. J FISH DIS. 1985;8(3):289-98.

23. Rao KVK. Inhibition of DNA synthesis in primary rat hepatocyte cultures by malachite green: a new liver tumor promoter. Toxicol Lett. 1995;81(2):107-13.

24. Fil BA. Isotherm, kinetic, and thermodynamic studies on the adsorption behavior of malachite green dye onto montmorillonite clay. Part Sci Technol. 2016;34(1):118-26.

25. Ammann L, Bergaya F, Lagaly G. Determination of the cation exchange capacity of clays with copper complexes revisited. Clay Miner2005. p. 441.

26. Sonawane SH, Chaudhari PL, Ghodke SA, Parande MG, Bhandari VM, Mishra S, et al. Ultrasound assisted synthesis of polyacrylic acid–nanoclay nanocomposite and its application in sonosorption studies of malachite green dye. Ultrason Sonochem. 2009;16(3):351-5.

27. Chinoune K, Bentaleb K, Bouberka Z, Nadim A, Maschke U. Adsorption of reactive dyes from aqueous solution by dirty bentonite. Appl Clay Sci. 2016;123(Supplement C):64-75.

28. Javadi F, Tayebee R. Preparation and characterization of ZnO/nanoclinoptilolite as a new nanocomposite and studying its catalytic performance in the synthesis of 2-aminothiophenes via Gewald reaction. Microporous Mesoporous Mater. 2016;231(Supplement C):100-9.

29. Khenifi A, Bouberka Z, Sekrane F, Kameche M, Derriche Z. Adsorption study of an industrial dye by an organic clay. ADSORPTION. 2007;13(2):149-58.

30. Crini G, Badot P-M. Application of chitosan, a natural aminopolysaccharide, for dye removal from aqueous solutions by adsorption processes using batch studies: A review of recent literature. Prog Polym Sci. 2008;33(4):399-447.

31. Crini G, Peindy HN, Gimbert F, Robert C. Removal of C.I. Basic Green 4 (Malachite Green) from aqueous solutions by adsorption using cyclodextrin-based adsorbent: Kinetic and equilibrium studies. Sep Purif Technol. 2007;53(1):97-110.

32. Akkaya G, Özer A. Biosorption of Acid Red 274 (AR 274) on Dicranella varia: Determination of equilibrium and kinetic model parameters. Process Biochem. 2005;40(11):3559-68.

33. Anirudhan TS, Ramachandran M. Surfactant-modified bentonite as adsorbent for the removal of humic acid from wastewaters. Appl Clay Sci. 2007;35(3):276-81.

34. Bulut Y, Karaer H. Adsorption of Methylene Blue from Aqueous Solution by Crosslinked Chitosan/Bentonite Composite. J Dispersion Sci Technol. 2015;36(1):61-7.

35. Fil BA, Özmetin C. Adsorption of cationic dye from aqueous solution by clay as an adsorbent: Thermodynamic and kinetic studies. J Chem Soc Pak. 2012;34(4):896-906.

36. Ofomaja AE. Sorptive removal of Methylene blue from aqueous solution using palm kernel fibre: Effect of fibre dose. Biochem Eng J. 2008;40(1):8-18.

37. Lodeiro P, Herrero R, Sastre de Vicente ME. Thermodynamic and Kinetic Aspects on the Biosorption of Cadmium by Low Cost Materials: A Review. Environ Chem. 2006;3(6):400-18.

38. Wan Ngah WS, Ariff NFM, Hashim A, Hanafiah MAKM. Malachite Green Adsorption onto Chitosan Coated Bentonite Beads: Isotherms, Kinetics and Mechanism. CLEAN – Soil, Air, Water. 2010;38(4):394-400.

39. Ho YS, McKay G. A Comparison of Chemisorption Kinetic Models Applied to Pollutant Removal on Various Sorbents. PROCESS SAF ENVIRON. 1998;76(4):332-40.

40. Doulia D, Leodopoulos C, Gimouhopoulos K, Rigas F. Adsorption of humic acid on acid-activated Greek bentonite. J Colloid Interface Sci. 2009;340(2):131-41.

41. Giles CH, Smith D, Huitson A. A general treatment and classification of the solute adsorption isotherm. I. Theoretical. J Colloid Interface Sci. 1974;47(3):755-65.

42. Chen JP, Wu S, Chong K-H. Surface modification of a granular activated carbon by citric acid for enhancement of copper adsorption. CARBON. 2003;41(10):1979-86.

43. Tahir SS, Rauf N. Removal of a cationic dye from aqueous solutions by adsorption onto bentonite clay. CHEMOSPHERE. 2006;63(11):1842-8.